JOURNAL OF PHYSICAL ORGANIC CHEMISTRY
J. Phys. Org. Chem. 2002; **15:** 448–460
Published online in Wiley InterScience (www.interscience.wiley.com). DOI: 10.1002/poc.496

Review Commentary

Catalysis in electron transfer reactions: facts and mechanistic insights†

Shunichi Fukuzumi*

Department of Material and Life Science, Osaka University, CREST, Japan Science and Technology Corporation (JST), Suita, Osaka 565-0871, Japan

Received 27 September 2001; revised 28 December 2001; accepted 10 January 2002

ABSTRACT: Catalysis in electron transfer reactions between electron donors and acceptors is described and the important mechanistic insight is provided by showing a number of examples of both thermal and photochemical reactions that involve metal ion-catalyzed electron transfer processes as the rate-determining steps. The quantitative measure of Lewis acidity of metal ions was obtained from the g_{zz} values of ESR spectra of superoxide–metal ion complexes which vary significantly depending on the type of metal ions. Copyright © 2002 John Wiley & Sons, Ltd.

KEYWORDS: catalysis; electron transfer; metal ions; superoxide dismutase; oxygen; fullerene

INTRODUCTION

Catalysis is the most important concept to control any kind of chemical reactions, including enzymatic reactions in biological systems. Among many types of chemical reactions, an electron transfer reaction is the most fundamental, since the electron is the minimum unit of the change in chemical reactions and any chemical bond is formed via electrons. However, catalysis in electron transfer reactions has yet to emerge as an identifiable field of study. The conceptual lack of catalysis in electron transfer reactions may stem from the general belief that there may be no need for catalysis to accelerate further the electron transfer reaction which is generally fast enough in a practical sense. This is largely true for reversible electron transfer reactions in which electron transfer occurs only when the free energy change of electron transfer is negative, i.e. the electron transfer is exergonic. If the electron transfer is endergonic, no net electron transfer would occur because of facile back electron transfer to regenerate the reactant pair. However, numerous chemical reactions, previously formulated by 'movements of electron pairs,' are now understood as processes in which an initial electron transfer from a nucleophile (reductant) to an electrophile (oxidant) produces a radical ion pair, which leads to the final products via the follow-up steps involving cleavage and formation of chemical bonds.[1–6] The follow-up steps are usually sufficiently rapid to render the initial electron transfer the rate-determining step in an overall irreversible transformation. In such a case, catalysis in the rate-determining electron transfer step, which is usually endergonic ($\Delta G^\circ_{et} > 0$) and thereby thermodynamically unfavorable, would play an essential role in accelerating the overall redox reaction.

Since electron transfer is an elementary reaction step, the acceleration of the rate of electron transfer with a 'promoter' should involve a change in the driving force of electron transfer by binding of the promoter with a product of electron transfer. Strictly, such an acceleration effect of a 'promoter' on electron transfer should not be called catalysis, since a 'catalyst' should not be involved in the stoichiometry of the reaction. However, a 'promoter' becomes equivalent to a 'catalyst' when the promoted initial electron transfer is the rate-determining step in an overall irreversible transformation and the promoter is not involved in the final products. In any catalytic reaction, a catalyst should bind with a substrate in the rate-determining step in the overall reaction.

This paper is intended to focus on catalysis in both thermal and photoinduced electron transfer reactions between electron donors and acceptors by investigating the effects of metal ions that can reduce the activation barrier of electron transfer reactions. The term of 'catalysis' is used to mean the acceleration effect of rates of electron transfer which can be applied to the

**Correspondence to:* S. Fukuzumi, Department of Material and Life Science, Osaka University, CREST, Japan Science and Technology Corporation (JST), Suita, Osaka 565-0871, Japan.
E-mail: fukuzumi@ap.chem.eng.osaka-u.ac.jp
†Presented at the 8th European Symposium on Organic Reactivity (ESOR-8), Cavtat (Dubrovnik), Croatia, September 2001.
Contract/grant sponsor: Ministry of Education, Culture, Sports, Science and Technology, Japan.

overall redox reactions which involve the electron transfer as the rate-determining step. First a quantitative measure to determine the Lewis acidity of a variety of metal ions is introduced in relation to the catalytic reactivities of metal ions in electron transfer reduction of O_2. Then, a bimetallic catalytic system is shown in relation to the superoxide dismutase (SOD) mechanism. Although oxygen is normally an oxidant and not a catalyst, a novel example where O_2 acts as a catalyst in accelerating back electron transfer reactions of artificial photosynthetic reaction centers is presented to demonstrate the importance of binding of metal ions to $O_2^{\cdot-}$ in controlling electron transfer reactions. The mechanistic insight into catalysis in electron transfer is described by showing examples of redox reactions that involve catalyzed electron transfer processes as the rate-determining steps.

QUANTITATIVE MEASURE OF LEWIS ACIDITY OF METAL IONS

A variety of metal ions (M^{n+}) can form complexes with $O_2^{\cdot-}$.[7,8] The $O_2^{\cdot-}$–M^{n+} complexes can be produced by photoinduced electron transfer from the excited state of dimeric 1-benzyl-1,4-dihydronicotinamide [$(BNA)_2$], which can act as a unique two-electron donor,[9,10] to O_2 in the presence of metal ion in acetonitrile [Eqn. (1)].[8]

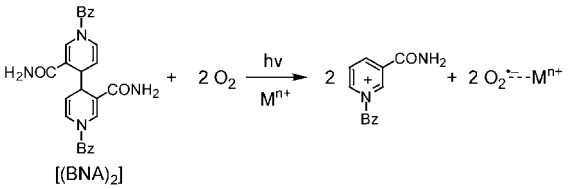

(1)

Addition of metal ions to the $(BNA)_2$–O_2 system results in the appearance of the anisotropic ESR signal measured at 143 K after irradiation with UV light as shown in Fig. 1.[8] The g_{zz} value of the $O_2^{\cdot-}$–M^{n+} complex varies depending on the type of metal ions. The g_{zz} value gives valuable information concerning the binding strength of the $O_2^{\cdot-}$–M^{n+} complex. The deviation of the g_{zz} value from the free spin value ($g_e = 2.0023$) is caused by the spin–orbit interaction as given by Eqn. (2) under the conditions that $\Delta E \gg \lambda$, where λ is the spin–orbit coupling constant (0.014 eV)[11] and ΔE is the energy splitting of π_g levels due to the complex formation between $O_2^{\cdot-}$ and M^{n+}.[12]

$$g_{zz} = g_e + 2\lambda/\Delta E \qquad (2)$$

The ΔE value is readily determined from the g_{zz} value using Eqn. (2). The ΔE value increases generally in the order monovalent cations (M^+) < divalent cations (M^{2+}) < trivalent cations (M^{3+}).[8] The ΔE value also increases with decreasing ion radius when the oxidation state of the metal ion is the same. Scandium ion, which has the smallest ion radius among the trivalent metal cations, gives the largest ΔE value. This indicates that the binding energy between Sc^{3+} and $O_2^{\cdot-}$ is the strongest among metal ions examined.[8]

The ΔE value can be used to predict the catalytic reactivities of M^{n+} in M^{n+}-catalyzed electron transfer from CoTPP (TPP = tetraphenylporphyrin dianion) to O_2 [Eqn. (3)] in acetonitrile at 298 K.[8,13]

$$\mathrm{CoTPP} + \mathrm{O_2} \xrightarrow[k_{cat}]{M^{n+}} \mathrm{CoTPP^+} + \mathrm{O_2^{\cdot-}} - \mathrm{M^{n+}} \qquad (3)$$

In the absence of metal ion, no electron transfer from CoTPP to O_2 occurs since the electron transfer is highly endergonic judging from the one-electron oxidation potential of CoTPP ($E^\circ_{ox} = 0.35$ V vs SCE in MeCN)[14] and the one-electron reduction potential of O_2 ($E^\circ_{red} = -0.87$ V vs SCE).[15] The catalytic effects of metal ions in electron transfer reduction of substrates have been ascribed to the binding of metal ions to the substrate radical anions produced in the electron transfer reactions.[6,16] Strictly, these are the 'promoting' effects and not the catalytic effects, since the metal ions bind with the products. However, a metal ion 'promoter' becomes a real 'catalyst' when the metal ion-promoted electron transfer is followed by the facile irreversible chemical steps in which the metal ion is removed from the final product as mentioned in the Introduction.

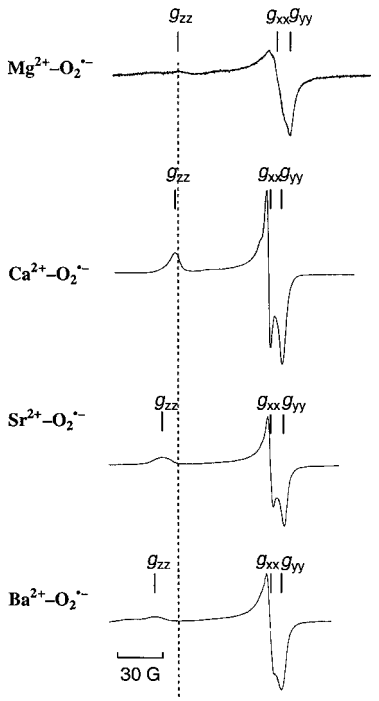

Figure 1. ESR spectra of M^{2+}–$O_2^{\cdot-}$ complexes (M^{2+} = Mg^{2+}, Ca^{2+}, Sr^{2+} and Ba^{2+}) in frozen MeCN at 143 K.[8] The vertical axis is the relative ESR intensity that is omitted

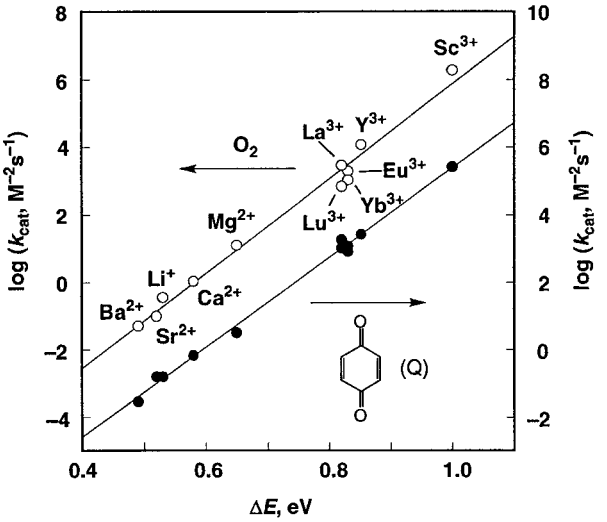

Figure 2. Plots of log k_{cat} vs ΔE in M^{n+}-catalyzed electron transfer from CoTPP to O_2 (○) and *p*-benzoquinone (●) in acetonitrile at 298 K[8]

There is a striking linear correlation between the catalytic rate constants (logk_{cat}) of electron transfer from CoTPP to O_2 and ΔE of the $O_2^{\cdot-}$–M^{n+} complex derived from the g_{zz} values as shown in Fig. 2 (open circles). The remarkable correlation spans a range of almost 10^7 in the rate constant. The slope of the linear correlation between logk_{cat} for M^{n+}-catalyzed electron transfer from CoTPP to O_2 and ΔE is obtained as 14.0 eV^{-1}, which is close to the value of $1/2.3RT$(= 16.9 eV^{-1}), where R is the gas constant and T = 298 K. Such a correlation has also been observed for the M^{n+}-catalyzed (promoted) electron transfer from CoTPP to *p*-benzoquinone (Q) as shown in Fig. 2 (open circles).[8] The slope (13.3) for Q is nearly the same as the slope (14.0) for O_2. This indicates that the variation of ΔE is well reflected in the difference in the activation free energy for the M^{n+}-catalyzed (promoted) electron transfer from CoTPP to not only O_2 but also Q. The stronger the binding of M^{n+} with $O_2^{\cdot-}$, the larger will be the catalytic effects of M^{n+}. Thus, ΔE can be regarded as good measure of the binding energies in the $O_2^{\cdot-}$–M^{n+} complexes, which is used as a quantitative measure of Lewis acidity of the metal ion.

CATALYTIC MECHANISM OF SOD

Superoxide ion is toxic, causing oxidative damage of cells, and is thus removed by copper zinc superoxide dismutase (Cu,Zn-SOD), which catalyzes the disproportionation (dismutation) of $O_2^{\cdot-}$ to O_2 and H_2O_2.[17–20] The important role of Zn(II) ion in the bimetallic system in activating both the oxidation and reduction of $O_2^{\cdot-}$ has been implicated by a well-characterized SOD model, an imidazolate-bridged Cu(II)–Zn(II) heterodinuclear complex containing a dinucleating ligand, Hbdpi [Hbdpi = 4,5-bis[di(2-pyridylmethyl)aminomethyl]imidazole].[21] The crystal structure is shown in Fig. 3.[21] The Cu(II)–Zn(II) distance of 6.197(2) Å in the Cu(II)–Zn(II) heterodinuclear complex agrees well with that of native Cu,Zn-SOD (6.2 Å), and each metal has pentacoordinate geometry with the imidazolate nitrogen, two pyridine nitrogens, the tertiary amine nitrogen and a solvent (MeCN or H_2O).[21] The ESR spectrum of complex of the Cu(II)–Zn(II) heterodinuclear complex gave well-defined ESR parameters ($g_{\|}$ = 2.10, $g_{\perp}$ = 2.24, $|A_{\|}|$ = 11.7 mT and $|A_{\perp}|$ = 12.4 mT), which indicate that the Cu(II) ion in the complex has a trigonal bipyramidal environment and a d_z^2 ground state following the criteria given by Bencini *et al.*[22] This agrees with the x-ray structure in Fig. 3.[21] The observation of a well-defined ESR spectrum also confirms that the complex retains its imidazolate-bridged Cu(II)–Zn(II) heterodinuclear structure and that it is not a 1:1 mixture of Cu(II)–Cu(II) and Zn(II)–Zn(II) homodinuclear complexes. The Cu(II)–Zn(II) SOD model complex has a coordination site available for the binding of superoxide ion (Fig. 3).

The Cu(II)–Zn(II) heterodinuclear complex exhibits catalytic activity towards the dismutation of superoxide anions. The SOD activity of the Cu(II)–Zn(II) heterodinuclear complex was investigated by the cytochrome *c* assay[23] using the xanthine oxidase reaction as the source of superoxide. The concentration of complex required to attain 50% inhibition of the reduction (defined as IC_{50}) was determined for the Cu(II)–Zn(II) heterodinuclear complex as 0.24 μM. This IC_{50} value corresponds to the highest activity among the structurally established SOD models reported so far.[21,23–26]

The cyclic voltammogram (CV) of the Cu(II)–Zn(II)

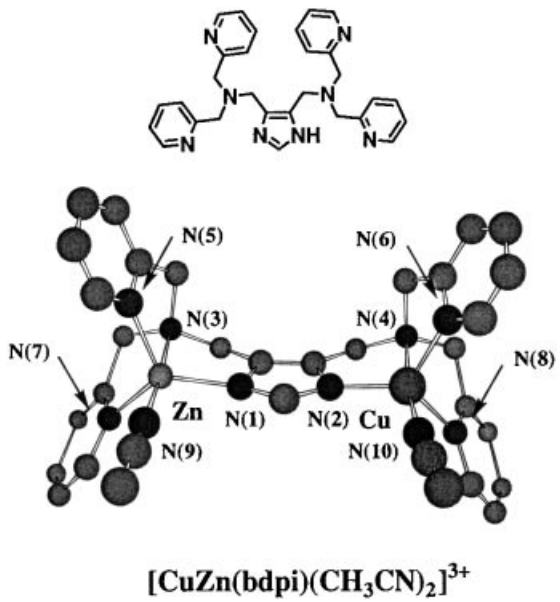

Figure 3. Crystal structure of $[Cu^{II}Zn^{II}(bdpi)(CH_3CN)_2](ClO_4)_3 \cdot 2CH_3CN$.[21] The hydrogen atoms are omitted for clarity

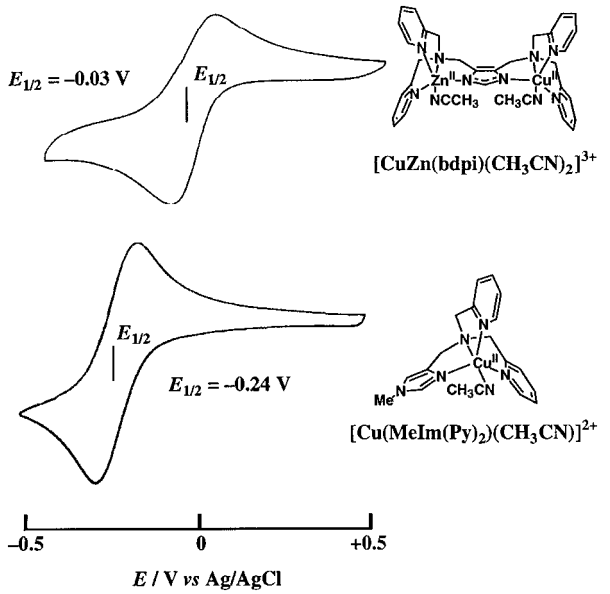

Figure 4. Cyclic voltammograms of $CuZn(bdpi)(CH_3CN)_2](ClO_4)_3$ and $[Cu(MeIm(Py)_2(CH_3CN)](ClO_4)_2$ (1.0 mM) in acetonitrile containing 0.1 M n-BuN_4ClO_4. Working electrode, glassy carbon; counter electrode, Pt wire; reference electrode, Ag/AgCl; scan rate, 50 mV s^{-1} [21]

heterodinuclear complex in acetonitrile is shown in Fig. 4, where the CV of the Cu(II) mononuclear complex, $[Cu(MeIm(Py)_2(CH_3CN)]ClO_4$, is also shown for comparison.[21] The CV of the Cu(II)–Zn(II) heterodinuclear complex exhibits only one reversible Cu(II)/(I) redox couple at $E_{1/2}$ = -0.03 V (vs. Ag/AgCl). This also confirms that complex contains one copper ion site. A comparison of the $E_{1/2}$ values between the Cu(II)–Zn(II) heterodinuclear complex and the corresponding Cu(II) mononuclear complex in Fig. 4 reveals that the $E_{1/2}$ value of the Cu(II)–Zn(II) heterodinuclear complex is 0.21 V more positive than the value of the Cu(II) mononuclear complex. Such a positive shift of the $E_{1/2}$ value of the Cu(II)–Zn(II) heterodinuclear complex can be ascribed to the electronic effect of the imidazolate-bound Zn(II) ion, which leads to a decrease in the electron density on the copper ion. This indicates that an important role of Zn(II) ion in the imidazolate-bridged Cu(II)–Zn(II) complex is to accelerate an outer-sphere electron transfer from $O_2^{\cdot -}$ to produce the Cu(I)–Zn(II) complex, when the free energy change of electron transfer becomes thermodynamically more favorable compared with that without Zn(II) ion.

Zn(II), which can act as a Lewis acid, is also able to accelerate an electron transfer from the Cu(I)–Zn(II) complex to $O_2^{\cdot -}$, since $O_2^{\cdot -}$ can form a complex with metal ions acting as a Lewis acid to accelerate the electron transfer reduction of $O_2^{\cdot -}$ (see above).[8] Such an acceleration for the reduction of $O_2^{\cdot -}$ can also be attained by a Brønsted acid instead of a Lewis acid since Valentine and co-workers reported that the reduction of $O_2^{\cdot -}$ for the zinc-deficient SOD form is acid-catalyzed.[27] The formation of an $O_2^{\cdot -}$–Zn(II) complex is confirmed using Zn(II) complexes, $[Zn^{II}[MeIm(Py)_2](CH_3CN)](ClO_4)_2$ and $[Zn^{II}[MeIm(Me)_2](CH_3CN)](ClO_4)_2$ [MeIm(Py)$_2$ = (1-methyl-4-imidazolylmethyl)bis(2-pyridylmethyl)amine, MeIm(Me)$_2$ = (1-methyl-4-imidazolylmethyl)bis(6-methyl-2-pyridylmethyl)amine], as shown in Eqn. (4):[28,29]

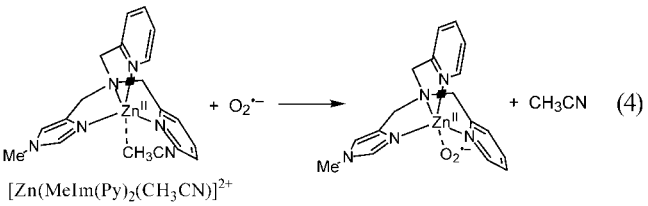

The ESR spectra of the Zn(II)–$O_2^{\cdot -}$ complexes measured at 133 K gave g_{zz} values which are significantly smaller than the value for free $O_2^{\cdot -}$ owing to the complexation of Zn(II) ion with $O_2^{\cdot -}$.[28,29] The ΔE values of the Zn(II)–$O_2^{\cdot -}$ complexes have been evaluated from deviation of the g_{zz} values from the free spin value. The ΔE values of the $O_2^{\cdot -}$ complex with $[Zn^{II}[MeIm(Me)_2]]^{2+}$ (0.87 eV) and $[Zn^{II}[MeIm(Py)_2]]^{2+}$ (0.85 eV) are significantly larger than those of $O_2^{\cdot -}$ complexes with other divalent metal ions [Mg(II) ion, 0.65 eV; Ca(II) ion, 0.58 eV; Sr(II) ion, 0.52 eV; and Ba(II) ion, 0.49 eV],[8] reflecting the strong Lewis acidity of Zn(II) ion compared with other divalent metal ions.[28,29] Thus, the essential role of Zn(II) ion in SODs is to accelerate both the oxidation and reduction of superoxide ion by controlling the redox potentials of Cu(II) ion and superoxide ion in the catalytic cycle of SOD as shown in Scheme 1. In the case of outer-sphere electron transfer from $O_2^{\cdot -}$ to the Cu(I)–Zn(II) complex, there is no need for interaction between $O_2^{\cdot -}$ and the Cu(I)–Zn(II) complex. In contrast, the binding of $O_2^{\cdot -}$ with Zn(II) is essential for electron transfer from Cu(I) to $O_2^{\cdot -}$. A similar effect is also expected for another copper ion in the Cu(II)–Cu(II) homodinuclear complex contain-

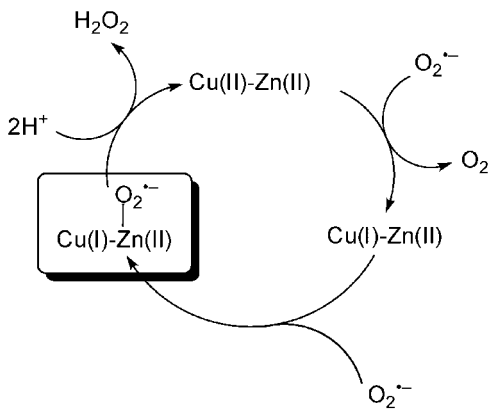

Scheme 1. Catalytic mechanism of SOD

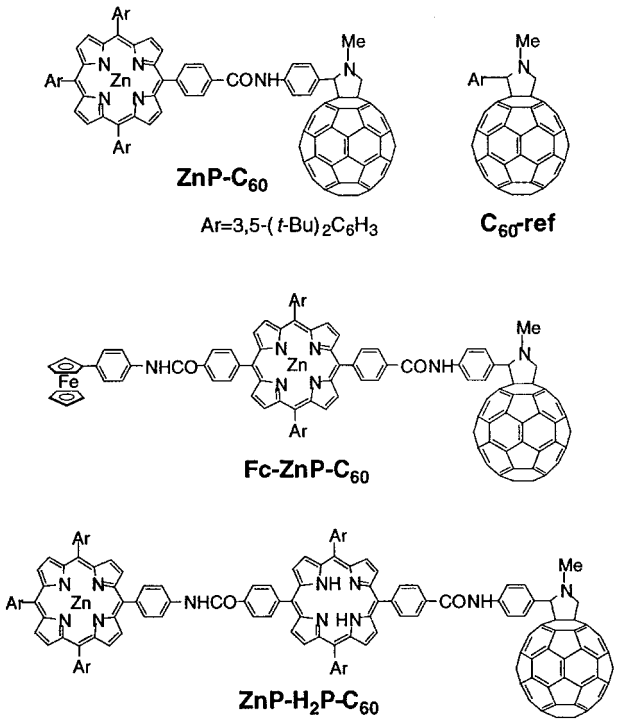

Figure 5. Structures of zinc porphyrin–fullerene linked compounds[35]

ing the same Hbdpi ligand.[21] The same mechanism as in Scheme 1 can be applied to the disproportionation of semiquinone radical anion by the imidazolate-bridged Cu(II)–Zn(II) complex.[30] The Zn(II) ion also plays an essential role in facilitating the reduction of semiquinone radical anion by coordination of the radical anion to the Zn(II) ion.[30]

CATALYSIS OF OXYGEN IN ELECTRON TRANSFER

Photoinduced electron transfer reactions of porphyrin-containing donor–acceptor linked systems have been extensively studied in order to mimic the photosynthetic process.[31–34] Extensive efforts have been directed towards achieving long-lived photoinduced charge separation by changing the redox properties of the donor and acceptor moieties and the distance of the donor–acceptor pair which is covalently linked, since the electron transfer rates are determined by these factors.[31–34] Thus, the rate of electron transfer is automatically determined and it cannot be changed once a donor–acceptor pair is fixed. However, there are now a number of examples for photoinduced electron transfer reactions which are accelerated significantly by the presence of a third component acting as a catalyst.[6,16] A simple molecule, such as dioxygen, has been shown to be employed as a powerful catalyst in accelerating the back electron transfer (BET) from a fullerene radical anion to a zinc porphyrin radical cation within photolytically generated radical ion pairs.[35] This is the first example in which O_2, the most important biological oxidant, acts as a catalyst rather than an oxidant in BET reactions. Coordination of $O_2^{\cdot-}$ to Zn(II) ion plays an important role not only in the catalytic function of Cu,Zn-SOD (Scheme 1) but also in the novel catalytic effect of O_2 in BET from a fullerene radical anion to a zinc porphyrin moiety within photolytically generated radical ion pairs of zinc porphyrin-fullerene linked molecules shown in Fig. 5.[35]

These zinc porphyrin–fullerene linked dyad and triads have been developed as artificial photosynthetic systems which, upon photoexcitation, give rise to long-lived charge-separated states in high quantum yields.[35,36] The energy levels in benzonitrile are shown in Scheme 2 to illustrate the different relaxation pathways of photoexcited **ZnP–C_{60}**.[35,36] The charge-separated state is obtained from the photoinduced electron transfer involving the singlet and triplet excited states of ZnP and C_{60} and decays via the back electron transfer from $C_{60}^{\cdot-}$ to $ZnP^{\cdot+}$. Each step in Scheme 2 can be monitored by time-resolved techniques, including fluorescence lifetime and

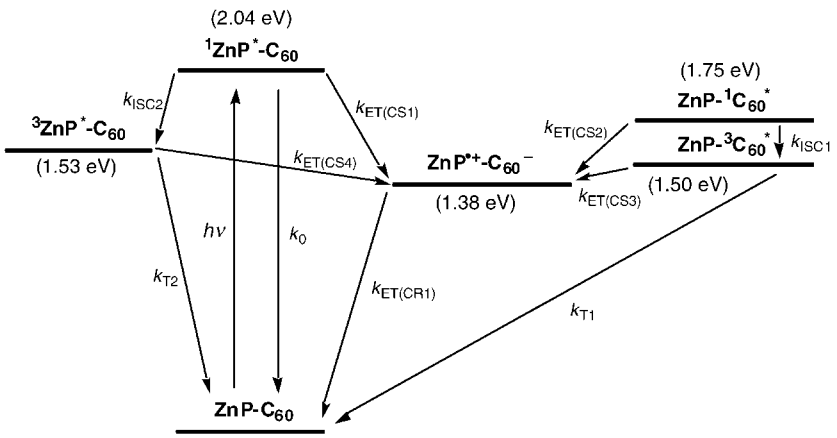

Scheme 2. Energy diagram of **ZnP–C_{60}**

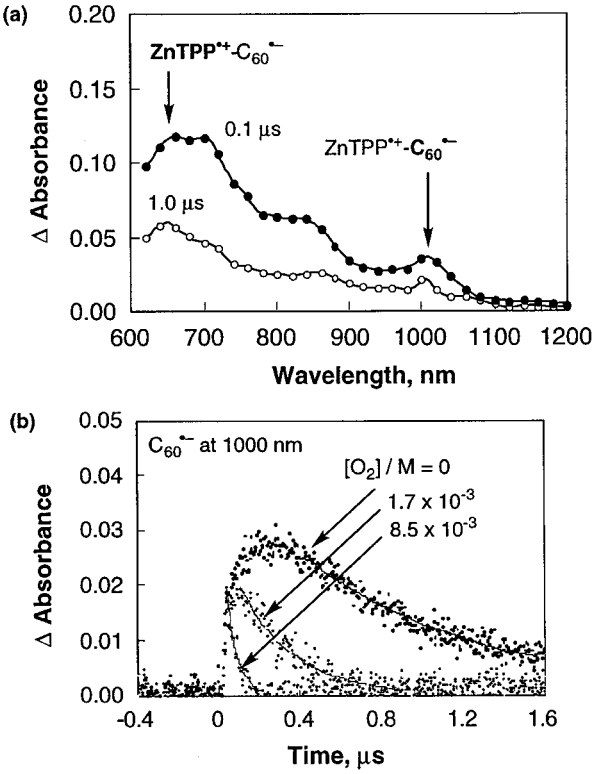

Figure 6. (a) Transient absorption spectra for **ZnP–C$_{60}$** after laser excitation (0.10 and 1.0 μs) in the absence of O_2 in PhCN.[35] (b) Time profiles of the absorbance at 1000 nm due to $C_{60}^{\cdot-}$ in **ZnP$^{\cdot+}$–C$_{60}^{\cdot-}$** in the absence and presence of O_2 in PhCN [35]

transient absorption measurements, disclosing the crucial formation of ZnP$^{\cdot+}$–*spacer*–$C_{60}^{\cdot-}$ and Fc^+–*spacer*–$C_{60}^{\cdot-}$ pairs in a variety of solvents.[35,36] For example, a deoxygenated benzonitrile (PhCN) solution containing **ZnP–C$_{60}$** gives rise upon a 532 nm laser pulse to a characteristic absorption spectrum with maxima at 650 and 1000 nm [Fig. 6(a)].[35] While the former maximum (650 nm) is a clear attribute of the ZnP$^{\cdot+}$, the latter maximum (1000 nm) corresponds to the diagnostic marker of the fullerene radical anion.[37] The decay of both absorption bands obeys clear first-order kinetics. This indicates an intramolecular BET from $C_{60}^{\cdot-}$ to ZnP$^{\cdot+}$ governs the fate of the **ZnP$^{\cdot+}$–C$_{60}^{\cdot-}$** radical ion pair. In the presence of O_2, the decay rate of both $C_{60}^{\cdot-}$ and ZnP$^{\cdot+}$ absorption is markedly accelerated compared with that found in the absence of O_2 [Fig. 6(b)]. The decay rate of $C_{60}^{\cdot-}$ coincides with that of ZnP$^{\cdot+}$ and increases linearly with increasing O_2 concentration.[35]

In contrast to the **ZnP–C$_{60}$** dyad, the k_{BET} value from $C_{60}^{\cdot-}$ to ferricenium ion (Fc^+) in **Fc$^+$–ZnP–C$_{60}^{\cdot-}$** was not affected by the presence of O_2.[35] The smaller k_{BET} value of the triad (**Fc–ZnP–C$_{60}$**: 1.3×10^5 s^{-1}) compared with that of the dyad (**ZnP–C$_{60}$**: 1.3×10^6 s^{-1}) stems from the larger edge-to-edge distance of the former ($R_{ee} = 30.3$ Å)[38] relative to the latter ($R_{ee} = 11.9$ Å).[39,40] Although an even smaller k_{BET} value (4.8×10^4 s^{-1}) was noted for the BET dynamics from $C_{60}^{\cdot-}$ to ZnP$^{\cdot+}$ in the **ZnP$^{\cdot+}$–H$_2$P–C$_{60}^{\cdot-}$** triad, the k_{BET} value is, nevertheless, expedited with increasing O_2 concentration. Thus, the presence of ZnP$^{\cdot+}$ appears essential for the accelerating effect of O_2 on the decay of the radical ion pair. The energy transfer pathway from **ZnP$^{\cdot+}$–C$_{60}^{\cdot-}$** via **ZnP–^{3}C$_{60}$*** has been ruled out as a major contributor to the decay of the radical ion pair, since much smaller intensity of $^1\Delta_g$ O_2 phosphorescence of the **ZnP–C$_{60}$** system is observed compared with **C$_{60}$**–ref 35.

The electron transfer from $C_{60}^{\cdot-}$ to O_2 is endergonic [$\Delta G^\circ_{et} \gg 0$ (0.28 eV)], judging from the one-electron reduction potentials of both species: E°_{red} of O_2 (−1.33 V vs Fc/Fc$^+$) is significantly lower than that of **C$_{60}$–ref** (−1.05 V vs Fc/Fc$^+$).[35] Thus, a direct electron transfer from $C_{60}^{\cdot-}$ in **ZnP$^{\cdot+}$–$C_{60}^{\cdot-}$** to O_2 is highly unlikely to occur in benzonitrile. In addition, the concomitant decay of ZnP$^{\cdot+}$ and $C_{60}^{\cdot-}$ in Fig. 6(a) is inconsistent with a direct electron transfer from $C_{60}^{\cdot-}$ to O_2, which would yield stable **ZnP$^{\cdot+}$–C$_{60}$** and $O_2^{\cdot-}$ on the present time-scale. The catalytic participation of O_2 in an intramolecular BET between $C_{60}^{\cdot-}$ and ZnP$^{\cdot+}$ in ZnP-linked C_{60} is depicted in Scheme 3. The intermolecular ET from $C_{60}^{\cdot-}$ to O_2 is made possible by the coordination of $O_2^{\cdot-}$ to ZnP$^{\cdot+}$, followed by a rapid intramolecular ET from $O_2^{\cdot-}$ to ZnP$^{\cdot+}$ in the $O_2^{\cdot-}$–ZnP$^{\cdot+}$ complex to regenerate O_2 (Scheme 3). In the presence of metal ions, $O_2^{\cdot-}$ is known to coordinate to the metal ion, yielding the corresponding $O_2^{\cdot-}$–metal ion complex as described above.[8] The binding energy of $O_2^{\cdot-}$ with Zn(II) ion (ca 0.9 eV)[28] is sufficient to make an electron transfer from $C_{60}^{\cdot-}$ to O_2 energetically feasible. In contrast to the ZnP-containing donor–acceptor systems, ferrocene is a fully coordinated complex, omitting the coordination of another ligand, such as $O_2^{\cdot-}$. This is the reason for the lack of accelerating effects in the **Fc$^+$–ZnP–C$_{60}^{\cdot-}$** system.

The second-order rate constant of **ZnP$^{\cdot+}$–C$_{60}^{\cdot-}$** (1.6×10^9 M^{-1} s^{-1}) obtained from the linear dependence of k_{BET} on [O_2] in PhCN is only slightly lower than the diffusion-controlled limit in PhCN (5.6×10^9 M^{-1} s^{-1}).[35] On the other hand, the corresponding value for **ZnP$^{\cdot+}$–H$_2$P–C$_{60}^{\cdot-}$** (3.3×10^7 M^{-1} s^{-1}) is 48 times smaller than the value for **ZnP$^{\cdot+}$–C$_{60}^{\cdot-}$**. This k_{ET} ratio (48) is consistent with the k_{BET} ratio (27) (i.e. from $C_{60}^{\cdot-}$ to ZnP$^{\cdot+}$) between the triad and the dyad in the absence of

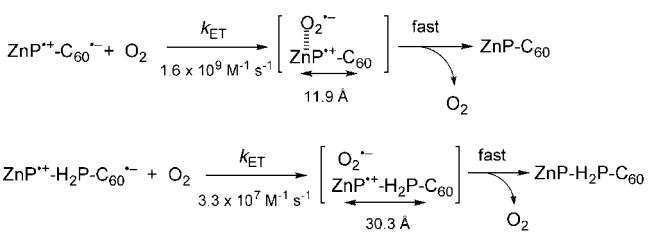

Scheme 3. Catalytic mechanism of O_2 in electron transfer

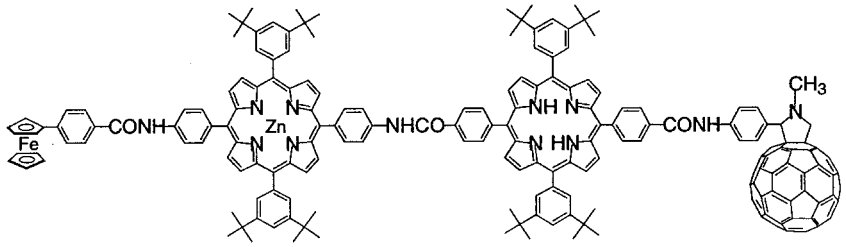

Fc-ZnP-H_2P-C_{60}

Figure 7. Structure of porphyrin–fullerene linked tetrad which achieves an extremely long-lived charge separated state[41]

O_2.[35] Thus, ET from $\mathbf{ZnP}^{\cdot+}$**–$\mathbf{H_2P}$–$\mathbf{C_{60}}^{\cdot-}$** to O_2 occurs even at a longer distance compared with ET from the $\mathbf{ZnP}^{\cdot+}$**–$\mathbf{C_{60}}^{\cdot-}$** dyad, since O_2 is placed at a longer distance from $C_{60}^{\cdot-}$ in the precursor complex for the electron transfer from $C_{60}^{\cdot-}$ to O_2 in $\mathbf{ZnP}^{\cdot+}$**–$\mathbf{H_2P}$–$\mathbf{C_{60}}^{\cdot-}$** (Scheme 3). In this way, O_2 acts as a novel catalyst to expedite intramolecular BET in ZnP-linked C_{60} systems where $ZnP^{\cdot+}$ accelerates an electron transfer from $C_{60}^{\cdot-}$ to O_2 and, thus, activates the catalysis of O_2 in the overall BET from $C_{60}^{\cdot-}$ to $ZnP^{\cdot+}$ (Scheme 3).

An extremely long-lived charge-separated state has been achieved successfully by extending the ferrocene containing triad (**Fc^+–ZnP–C_{60}**) to a ferrocene (**Fc**)–zincporphyrin (**ZnP**)–freebaseporphyrin **(H_2P)–C_{60}** tetrad (**Fc–ZnP–H_2P–C_{60}**) (Fig. 7), which reveals a cascade of photoinduced energy transfer and multistep electron transfer within a molecule in frozen media and in solutions.[41] The lifetime of the resulting charge-separated state (i.e. ferricenium ion–C_{60} radical anion pair) in frozen benzonitrile is determined as 0.38 s, which is more than one order of magnitude longer than any other intramolecular charge recombination processes of synthetic systems, and is comparable to that observed for the bacterial photosynthetic reaction center.[41]

CYCLOADDITION VS HYDRIDE TRANSFER VIA METAL ION-CATALYZED ELECTRON TRANSFER

The effects of metal ions on hydride transfer reactions from NADH analogues to substrates have attracted considerable interest in relation to the essential role of metal ions in the redox reactions of nicotinamide coenzymes in the native enzymatic system.[42–44] A hydride transfer from 1-benzyl-1,4-dihydronicotinamide (BNAH), employed as an NADH model compound, to *p*-benzoquinone (Q) proceeds via an electron transfer from BNAH to Q, followed by proton transfer from $BNAH^{\cdot+}$ to $Q^{\cdot-}$ and subsequent rapid electron transfer from the deprotonated radical ($BNA^{\cdot}$) to $QH^{\cdot}$ to give BNA^+ and QH^-.[45] The initial electron transfer step is accelerated by the presence of Mg^{2+}.[45] When BNAH is replaced by 1-benzyl-4-tert-butyl-1,4-dihydronicotinamide (*t*-BuBNAH), no reaction occurs between *t*-BuBNAH and Q in deaerated MeCN. In the presence of $Sc(OTf)_3$, however, cycloaddition reaction of *t*-BuBNAH with Q rather than hydride transfer occurs efficiently at 298 K [Eqn. (5)].[46]

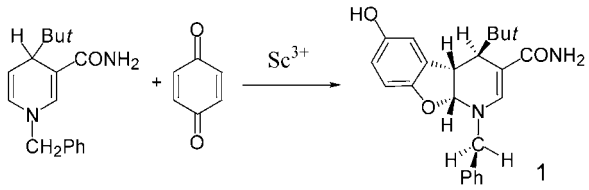

(5)

The cycloadduct **1** was isolated and a single crystal of **1** was obtained for x-ray crystal structure determination. An ORTEP drawing of **1** is shown in Fig. 8.

The rates of reactions of *t*-BuBNAH with Q in the presence of Sc^{3+} in MeCN at 298 K obeyed pseudo-first-order kinetics in the presence of large excess Q and Sc^{3+} relative to the concentration of *t*-BuBNAH. The pseudo-first-order rate constant increases proportionally with Q

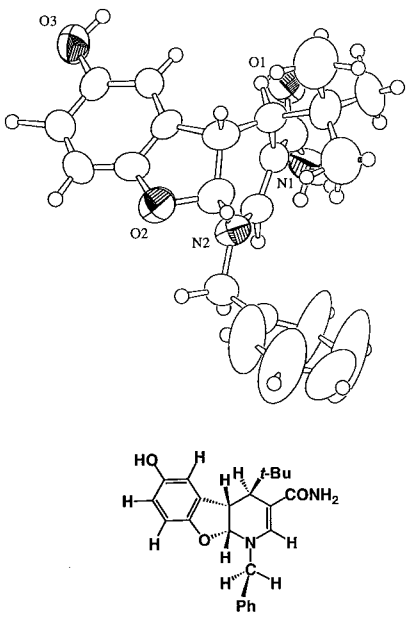

Figure 8. ORTEP drawing of the cycloadduct **1**[46]

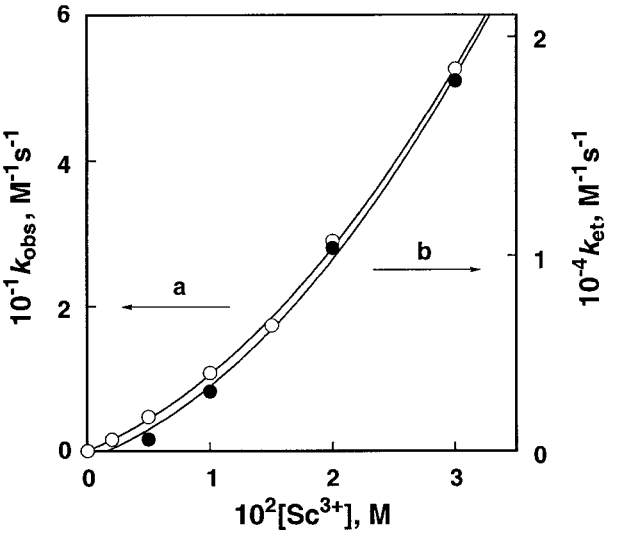

Figure 9. Dependence of k_{obs} on $[Sc^{3+}]$ for (a) the cycloaddition reaction of *t*-BuBNAH (1.0×10^{-4} M) with *p*-benzoquinone (2.0×10^{-3} M) and (b) electron transfer from CoTPP (8.0×10^{-6} M) to *p*-benzoquinone (2.6×10^{-4} M) in the presence of $Sc(OTf)_3$ in deaerated MeCN at 298 K [46]

concentration. Thus, the rate exhibits second-order kinetics showing a first-order dependence on each reactant concentration. The dependence of the observed second-order rate constant (k_{obs}) on $[Sc^{3+}]$ is shown in Fig. 9(a) for the cycloaddition reactions of *t*-BuBNAH with Q at various concentrations of Sc^{3+}. The k_{obs} value increases with an increase in $[Sc^{3+}]$ to exhibit a first-order dependence on $[Sc^{3+}]$ at low concentrations, changing to a second-order dependence at high concentrations.

Such a mixture of first- and second-order dependences on $[Sc^{3+}]$ is also observed in electron transfer from CoTPP to Q. No electron transfer from CoTPP to Q occurred in MeCN at 298 K. In the presence of $Sc(OTf)_3$, however, an efficient electron transfer from CoTPP to Q occurs to yield $CoTPP^+$ [Eqn. (6)];[8,46]

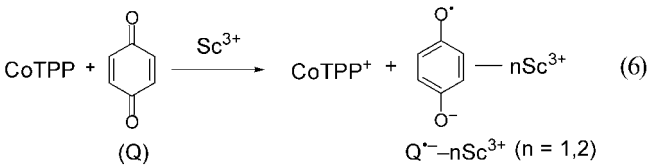

(6)

The electron-transfer rates also obeyed second-order kinetics, showing a first-order dependence on each reactant concentration. The dependence of the observed electron transfer rate constant (k_{et}) on $[Sc^{3+}]$ is also shown in Fig. 9(b), where the k_{et} value increases linearly with $[Sc^{3+}]$ to show a first-order dependence on $[Sc^{3+}]$ at low concentrations, changing to a second-order dependence at high concentrations as the case with the Sc^{3+}-catalyzed cycloaddition of *t*-BuBNAH with Q in Fig. 9(a).

There is no interaction between Q and Sc^{3+}, as indicated by the lack of spectral change of Q in the presence of Sc^{3+}.[46] In such a case, the acceleration of electron transfer from CoTPP to Q is ascribed to the complexation of Sc^{3+} with $Q^{\bullet-}$. Since there are two carbonyl oxygens which can interact with Sc^{3+}, $Q^{\bullet-}$ may form not only a 1:1 complex [$n = 1$ in Eqn. (3)] but also a 1:2 complex [$n = 2$ in Eqn. (3)] with Sc^{3+}. The complex formation between $Q^{\bullet-}$ and Sc^{3+} should result in a positive shift of the one-electron reduction potential of Q (E_{red}) and the Nernst equation is given by

$$E_{red} = E^0{}_{red} + (2.3RT/F)\log K_1[Sc^{3+}](1 + K_2[Sc^{3+}]) \quad (7)$$

where $E^0{}_{red}$ is the one-electron reduction potential of Q in the absence of Sc^{3+} and K_1 and K_2 are the formation constants for the 1:1 and 1:2 complexes between $Q^{\bullet-}$ and Sc^{3+}, respectively. Since Sc^{3+} has no effect on the oxidation potential of CoTPP, the free energy change of electron transfer from CoTPP to Q in the presence of Sc^{3+} (ΔG_{et}) can be expressed by

$$\Delta G_{et} = \Delta G^0{}_{et} - (2.3RT)\log(K_1[Sc^{3+}] + K_1K_2[Sc^{3+}]^2) \quad (8)$$

where $\Delta G^0{}_{et}$ is the free energy change in the absence of Sc^{3+}. Thus, electron transfer from CoTPP to Q becomes more favorable energetically with an increase in concentration of Sc^{3+}. If such a change in the energetics is directly reflected in the transition state of electron transfer, the dependence of the observed rate constant of electron transfer (k_{et}) on $[Sc^{3+}]$ is derived from Eqn. (8), as given by

$$k_{et} = k_0K_1[Sc^{3+}](1 + K_2[Sc^{3+}]) \quad (9)$$

where k_0 is the rate constant in the absence of Sc^{3+}. This equation predicts a first-order dependence on $[Sc^{3+}]$ at low concentrations, changing to a second-order dependence at high concentrations as observed experimentally [Fig. 9(b)]. The validity of Eqn. (9) is confirmed by the linear plot of $k_{et}/[Sc^{3+}]$ vs $[Sc^{3+}]$ for the Sc^{3+}-catalyzed electron transfer from CoTPP to Q. From the slopes and intercepts are obtained the K_2 values, which are listed in Table 1 together with the k_0K_1 values.

There is a striking similarity with respect to the dependence of k_{et} (or k_{obs}) on $[Sc^{3+}]$ between the electron transfer reactions from CoTPP to Q [Fig. 9(a)] and the cycloaddition reaction of *t*-BuBNAH with Q [Fig. 9(b)], despite the large difference in their reactivities. Thus, the same plot as in Eqn. (9) for the Sc^{3+}-catalyzed electron transfer from CoTPP to Q can be applied for the Sc^{3+}-catalyzed cycloaddition reactions of *t*-BuBNAH with Q.

Table 1. Rate constants (k_0K_1) of Sc^{3+}-catalyzed cycloaddition reactions of NADH analogues with *p*-benzoquinone derivatives (X–Q) and the formation constants (K_2) of the X–$Q^{\cdot-}$–$2Sc^{3+}$ complexes in deaerated acetonitrile at 298 K[a46]

NADH analogue	X–Q	k_0K_1[b] ($M^{-2}s^{-1}$)	K_2[b] (M^{-1})
t-BuBNAH	Q	7.3×10^2 (2.7×10^5)	4.6×10 (4.0×10)
i-PrBNAH	Q	4.7×10^3 (2.7×10^5)	4.9×10 (4.0×10)
BNAH	Q	1.3×10^4 (2.7×10^5)	4.9×10 (4.0×10)
BNAH	2,5-Cl_2Q	2.2×10^2 (9.3×10^5)	2.6×10 (2.5×10)
BNAH	2,5-Me_2Q	6.6×10 (1.1×10^5)	4.8×10 (4.3×10)
BNAH	2,6-Me_2Q	1.0×10 (8.0×10^4)	4.3×10 (4.7×10)

[a] K_1 and K_2 are the formation constants for the 1:1 and 1:2 complexes between $Q^{\cdot-}$ and Sc^{3+}, respectively; k_0 is the rate constant in the absence of Sc^{3+} (see text).
[b] Determined from the dependence of k_{obs} on [Sc^{3+}] based on Eqn. (9). The experimental error is 10%. Values in parentheses are those determined for Sc^{3+}-promoted electron transfer from CoTPP to X–Q.

The K_2 value for the 1:2 complex formation between $Q^{\cdot-}$ and Sc^{3+} is obtained from the linear plot of k_{obs}/[Sc^{3+}] vs [Sc^{3+}] as listed in Table 1. The dependence of k_{obs} on [Sc^{3+}] was also determined for the cycloaddition reactions of BNAH and *i*-PrBNAH with Q. The K_2 values were also determined from the linear plots of k_{obs}/[Sc^{3+}] vs [Sc^{3+}] and are listed in Table 1. These K_2 values (46–49 M^{-1}) are essentially the same within the experimental error irrespective of the different reactivities of NADH analogues (see k_0K_1 values in Table 1). In each case, the K_2 value agrees within experimental error with the value (40 M^{-1}) determined from the Sc^{3+}-promoted electron transfer reaction (Table 1). Such an agreement strongly indicates that the catalytic function of Sc^{3+} in the cycloaddition reactions of NADH analogues with Q is essentially the same as the function in electron transfer from CoTPP to Q. This means that the cycloaddition of the NADH analogues with Q proceeds via a rate-determining electron transfer from NADH analogues to Q, which is accelerated by formation of the 1:1 and 1:2 complexes between $Q^{\cdot-}$ and Sc^{3+} as in the case of an electron transfer from CoTPP to Q.

The K_2 values were also determined for other *p*-benzoquinone derivatives (X–Q) as listed in Table 1.[46] In each case, the K_2 value determined from the Sc^{3+}-catalyzed cycloaddition reactions with the *p*-benzoquinone derivative agrees with the value determined from the corresponding Sc^{3+}-promoted electron transfer reaction (Table 1). Such an agreement confirms that the Sc^{3+}-catalyzed cycloaddition of the NADH analogues with the *p*-benzoquinone derivative (X–Q) proceeds via the rate-determining Sc^{3+}-promoted electron transfer from NADH analogues to X–Q.

The 1:2 complex formation between $Q^{\cdot-}$ and Sc^{3+} was confirmed by observation of the ESR spectrum of the $Q^{\cdot-}$–$2Sc^{3+}$ complex, which shows the superhyperfine structure due to the interaction of $Q^{\cdot-}$ with two equivalent Sc nuclei. Since the $Q^{\cdot-}$–$2Sc^{3+}$ complex is unstable because of the facile disproportionation reaction, the complex was generated in photoinduced electron transfer from dimeric 1-benzyl-1,4-dihydronicotinamide [$(BNA)_2$] to Q at low temperatures. The observed ESR spectrum of $Q^{\cdot-}$ in the presence of Sc^{3+} is shown in Fig. 10.[46] The well-resolved 19 lines of the spectrum clearly indicate the hyperfine splitting [*a*(H)] due to four protons of semiquinone radical anions and superhyperfine splitting [*a*(Sc)] of two equivalent Sc^{3+} nuclei ($I = 7/2$). The coupling constants are almost the same between *a*(H) and *a*(Sc), resulting in the overall nuclear spin = 9, which causes 19 lines. The hyperfine coupling constants are determined as $a(H) = 1.15$ G, $a(Sc) = 1.15$ G with a linewidth (ΔH_{msl}) = 0.50 G. Thus, the observed ESR spectrum in Fig. 10 clearly demonstrates the formation of the 1:2 complex between $Q^{\cdot-}$ and Sc^{3+}.

When Sc^{3+} is replaced by weaker Lewis acids such as Lu^{3+} [$Lu(OTf)_3$], Y^{3+} [$Y(OTf)_3$] or Mg^{2+} [$Mg(ClO_4)_2$] in the reaction of *t*-BuBNAH with Q, BNA^+ is formed together with the cycloadduct (Table 2).[46] In the case of Mg^{2+}, the cycloaddition is no longer the main reaction but a hydride transfer from *t*-BuBNAH to Q occurs to yield *t*-BNA^+ as the major product (60%) (Table 2).[46] When *t*-BuBNAH is replaced by BNAH in the reaction with Q catalyzed by metal ions other than Sc^{3+}, a hydride

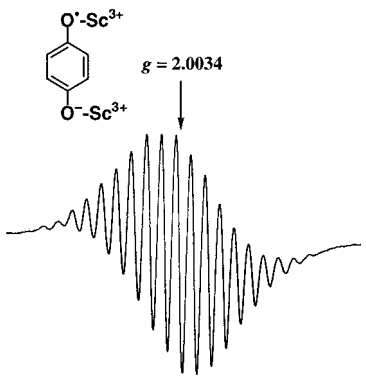

Figure 10. ESR spectrum of propionitrile solution containing $(BNA)_2$ (1.6×10^{-2} M), *p*-benzoquinone (4.9×10^{-2} M), and $Sc(OTf)_3$ (4.4×10^{-2} M) irradiated with a high-pressure mercury lamp at 203 K.[46] The vertical axis is the relative ESR intensity that is omitted

Table 2. Yields of products in reactions of BNAH and *t*-BuBNAH with *p*-benzoquinone in the presence of a metal ion [$Sc(OTf)_3$, $Lu(OTf)_3$, $Y(OTf)_3$ (0.1 M) or $Mg(ClO_4)_2$ (1.0 M)] and rate constants (k_{obs}) of reactions of *t*-BuBNAH (1.0×10^{-4} M) with *p*-benzoquinone (2.0×10^{-3} M) in the presence of metal ions (3.0×10^{-2} M) in deaerated acetonitrile at 298 K[46]

	Yield (%)					
	t-BuBNAH			BNAH		
Metal ion	Cycloadduct	BNA^+	*t*-$BuBNA^+$	Cycloadduct	BNA^+	$10^2\ k_{obs}$ ($M^{-1}\ s^{-1}$)
Sc^{3+}	100	0	0	100	0	5.3×10^3
Lu^{3+}	72	28	0	33	67	6.1
Y^{3+}	59	41	0	21	79	3.1
Mg^{2+}	35	5	60	7	93	0.26[a]

[a] $Mg(ClO_4)_2$ (0.5 M).

transfer from BNAH to Q becomes the main reaction and the yield of BNA^+ increases in the order Lu^{3+} (67%) < Y^{3+} (79%) < Mg^{2+} (93%) with a decrease in the Lewis acidity of the metal ion (Table 2).[46] The reaction mechanisms of Mg^{2+}-catalyzed hydride transfer from BNAH to Q have been extensively studied.[44,45,47] However, this is the first report disclosing the minor reaction pathway of the cycloaddition (7%) competing with the major hydride transfer reaction pathway (93%).[46]

The Mg^{2+}-catalyzed hydride transfer from BNAH to Q is known to proceed via an Mg^{2+}-promoted electron transfer from BNAH to Q, followed by a proton transfer from the resulting $BNAH^{\cdot+}$ to the $Q^{\cdot-}$–$2Mg^{2+}$ complex and subsequent fast electron transfer from $BNA^{\cdot}$ to QH^-–Mg^{2+}. The change in the type of reaction depending on the Lewis acidity of the metal ion (Table 2) is well accommodated in the electron transfer mechanism in Scheme 4.[46] The initial rate-determining electron transfer from *t*-BuBNAH to Q results in the formation of a radical ion pair (*t*-$BuBNAH^{\cdot+}$ and $Q^{\cdot-}$) where $Q^{\cdot-}$ forms 1:1 and 1:2 complexes with Sc^{3+}. This is followed by fast radical coupling between $Q^{\cdot-}$ and *t*-$BuBNAH^{\cdot+}$ to give the zwitterionic intermediate which is eventually converted to the cycloadduct **1**. In the same manner, the Sc^{3+}-catalyzed cycloaddition reaction of BNAH with Q proceeds via the Sc^{3+}-promoted electron transfer from BNAH to Q. The radical coupling of C(5) of $BNAH^{\cdot+}$ with $Q^{\cdot-}$–$2M^{n+}$ may occur efficiently [pathway (a)] in competition with the proton transfer from $BNAH^{\cdot+}$ to $Q^{\cdot-}$–$2M^{n+}$, which leads to the overall hydride transfer from BNAH to Q [pathway (c)]. With decreasing Lewis acidity of the metal ion, the metal ion-catalyzed electron transfer from BNAH to Q is decelerated because of the weaker binding of the metal ion with $Q^{\cdot-}$. On the other hand, the proton transfer from $BNAH^{\cdot+}$ to the $Q^{\cdot-}$–$2M^{n+}$ complex is accelerated with decreasing the Lewis acidity to the metal ion (M^{n+}) owing to the stronger basicity of the $Q^{\cdot-}$–$2M^{n+}$ complex. This may be the reason why the hydride transfer pathway from BNAH to Q becomes dominant in the presence of a much weaker Lewis acid (e.g. Mg^{2+}) compared with the selective cycloaddition reaction in the presence of Sc^{3+} (see the product yields in Table 2).

In the case of *t*-BuBNAH, the C(4)—C bond of *t*-$BuBNAH^{\cdot+}$ is known to be cleaved to produce *t*-$Bu^{\cdot}$,[48–50] which can combine with $Q^{\cdot-}$–$2M^{n+}$ [pathway (b) in Scheme 4], leading to the overall transfer of *t*-Bu^- to Q. With decreasing Lewis acidity of the metal ion, the C(4)—C bond cleavage of *t*-$BNAH^{\cdot+}$ may also be accelerated owing to the stronger basicity of the $Q^{\cdot-}$–$2M^{n+}$ complex. This may be the reason why the overall transfer of *t*-Bu^- to Q [pathway (b) in Scheme 4] starts to compete with the cycloaddition pathway as the Lewis acidity of the metal ion is decreased (see the product yields in Table 2). Thus, the Lewis acidity of metal ion can control not only the electron transfer step but also the subsequent chemical step.

SCANDIUM ION-CATALYZED PHOTOOXIDATION OF FULLERENES

The small reorganization energy of fullerenes, especially in electron transfer reactions, and the long triplet excited-state lifetimes, have rendered fullerenes useful components in the design of novel electron transfer systems in both the ground and excited states.[37,51–53] In comparison with the facile reduction of C_{60}, however, the oxidation of C_{60} is rendered more difficult with a reported one-electron oxidation potential of 1.26 V versus ferrocene/ferricenium.[54,55] Reed *et al.* have recently succeeded in oxidizing C_{60} by a strong one-electron oxidant (hexabrominated phenylcarbazole radical cation with inert $CB_{11}H_6X_6^-$ carborane anion) to produce stable $C_{60}^{\cdot+}$ in solution.[56] The use of an appropriate metal ion which can accelerate electron transfer reactions has removed the need for very strong oxidants to accomplish the electron transfer oxidation of fullerenes. In the presence of such a metal ion, a number of photoinduced electron transfer reactions, which would otherwise be unlikely to occur, are reported to proceed efficiently.[6,16,57,58]

In the presence of scandium triflate, an efficient photoinduced electron transfer from the triplet excited

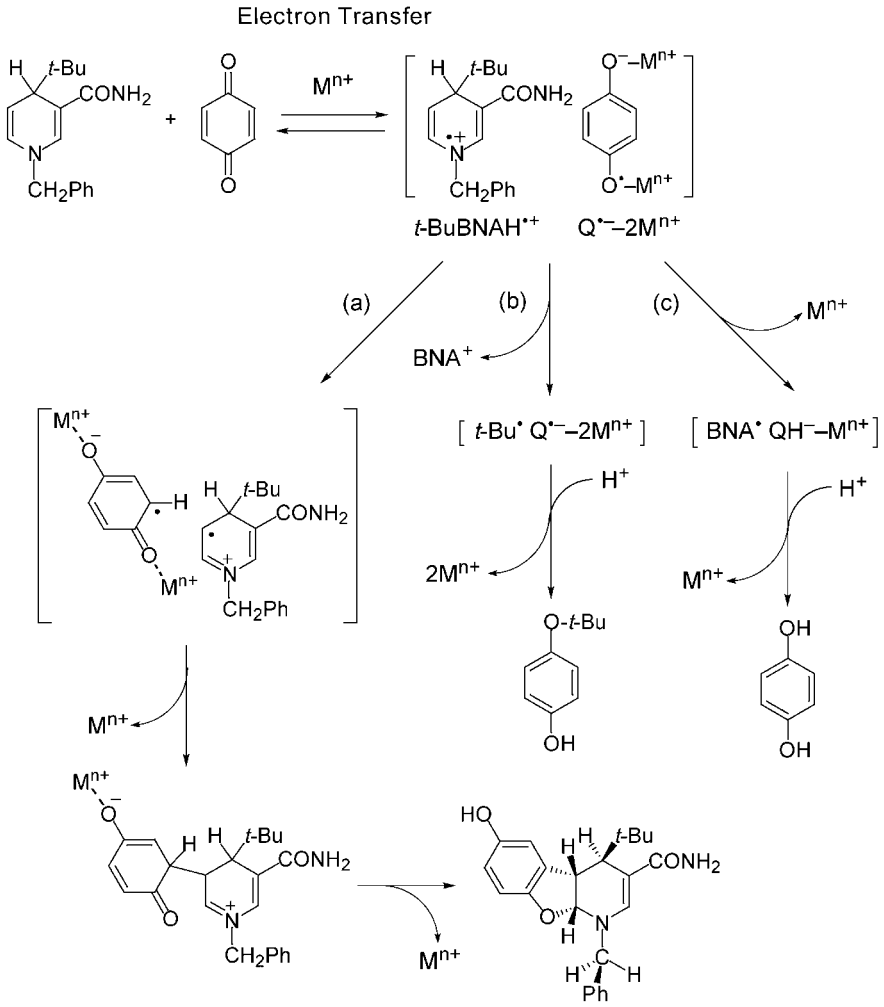

Scheme 4. Mechanism of Sc^{3+}-catalyzed reaction of *t*-BuBNAH with Q

state of C_{60} to *p*-chloranil occurs to produce C_{60} radical cation which has a diagnostic near-infrared absorption band at 980 nm, whereas no photoinduced electron transfer occurs from the triplet excited state of C_{60} ($^3C_{60}$*) to *p*-chloranil in the absence of scandium ion in benzonitrile, as shown in Fig. 11.[59] The electron transfer rate obeys pseudo-first-order kinetics and the pseudo-first-order rate constant increases linearly with increasing *p*-chloranil concentration.[54] The observed second-order rate constant of electron transfer (k_{et}) increases linearly with, increasing scandium ion concentration.[59] In contrast to the case of the C_{60}–*p*-chloranil–Sc^{3+} system, the k_{et} value for electron transfer from $^3C_{60}$* to *p*-benzoquinone increases with increase in Sc^{3+} concentration ([Sc^{3+}]) to exhibit a first-order dependence on [Sc^{3+}], changing to a second-order dependence at the high concentrations as observed in an Sc^{3+}-catalyzed electron transfer from CoTPP to *p*-benzoquinone (Fig. 9).[59] This is ascribed to the formation of 1:1 and 1:2 complexes between the generated semiquinone radical anion and Sc^{3+} at low and high concentrations of Sc^{3+}, respectively.

The Sc^{3+}-promoted photoinduced electron transfer oxidation of $^3C_{60}$* by *p*-chloranil can be applied for the formation of other fullerene radical cations.[59] The ESR spectra of the fullerene radical cations were also detected in frozen PhCN at 193 K under photoirradiation of the fullerene–*p*-chloranil–Sc^{3+} systems.[59] The *g* values and λ_{max} values of various fullerene radical cations thus determined are summarized in Fig. 12.[59]

CONCLUSION

It has been demonstrated that binding of a metal ion with the substrate radical anion plays an important role in controlling the electron transfer reactivity of the substrate. The binding energies of metal ions with $O_2^{\cdot -}$ derived from the g_{zz} values of ESR spectra of metal ion–$O_2^{\cdot -}$ complexes provide a quantitative measure of the Lewis acidity of metal ions in predicting the catalytic reactivities of metal ions in electron transfer reactions. The Lewis acidity of metal ions has been shown to

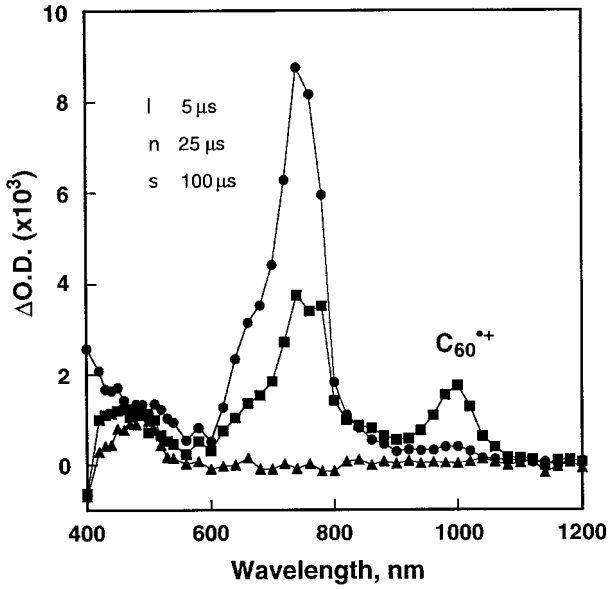

Figure 11. Transient absorption spectra observed in photoinduced electron transfer from C_{60} (1.1×10^{-4} M) to Cl_4Q (4.0×10^{-2} M) in the presence of Sc^{3+} (0.11 M) after laser irradiation at $\lambda = 532$ nm in deaerated PhCN at 298 K (●, 5 μs; ■, 25 μs; ▲, 100 μs)[59]

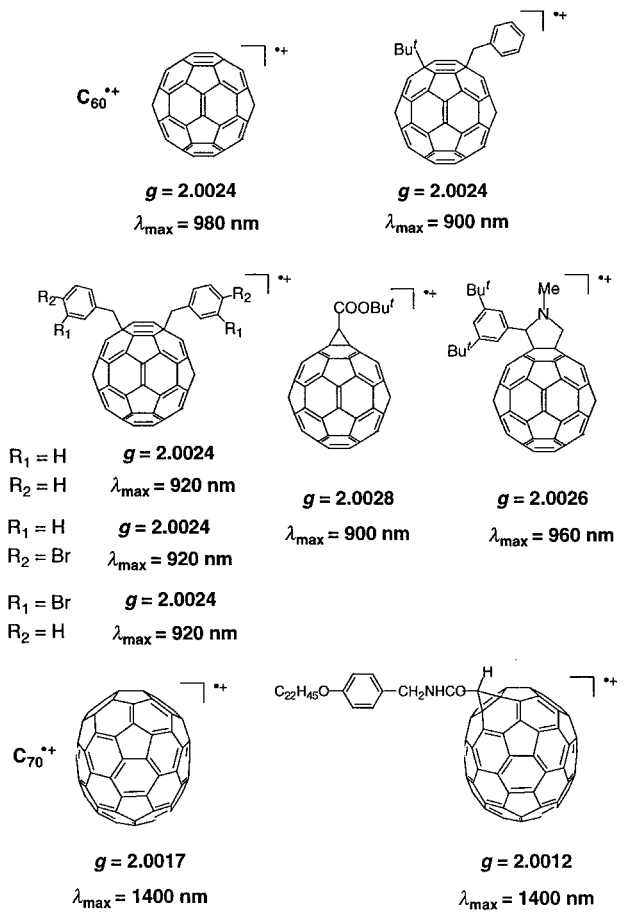

Figure 12. Structures, λ_{max} and g values of fullerene radical cations[59]

control not only the electron transfer step but also the subsequent chemical step in the overall redox reactions.

Acknowledgements

The author is deeply indebted to the work of all collaborators and co-workers whose names are listed in the references, in particular Professor H. Imahori, Professor O. Ito, Professor S. Itoh, Dr K. Ohkubo and Dr H. Ohtsu. S.F. acknowledges continuous support of the Ministry of Education, Culture, Sports, Science and Technology, Japan.

REFERENCES

1. Eberson L. *Electron Transfer Reactions in Organic Chemistry; Reactivity and Structure*, vol. 25. Springer: Heidelberg, 1987.
2. (a) Kochi JK. *Angew. Chem., Int. Ed. Engl.* 1988; **27**: 1227–1388; (b) Kochi JK. *Acc. Chem. Res.* 1992; **25**: 39–47; (c) Rathore R, Kochi JK. *Adv. Phys. Org. Chem.* 2000; **35**: 193–318.
3. Patz M, Fukuzumi S. *J. Phys. Org. Chem.* 1997; **10**: 129–137.
4. Astruc D. *Electron Transfer and Radical Processes in Transition Metal Chemistry*. VCH: New York, 1995.
5. Chanon M, Rajzmann M, Chanon F. *Tetrahedron* 1990; **46**: 6193–6299.
6. Fukuzumi S. In *Electron Transfer in Chemistry*, vol. 4, Balzani V (ed). Wiley-VCH: Weinheim, 2001; 3–67.
7. Fukuzumi S, Patz M, Suenobu T, Kuwahara Y, Itoh S. *J. Am. Chem. Soc.* 1999; **121**: 1605–1606.
8. Fukuzumi S, Ohkubo K. *Chem. Eur. J.* 2000; **6**: 4532–4535.
9. Fukuzumi S, Suenobu T, Patz M, Hirasaka T, Itoh S, Fujitsuka M, Ito O. *J. Am. Chem. Soc.* 1998; **120**: 8060–8068.
10. Patz M, Kuwahara Y, Suenobu T, Fukuzumi S. *Chem. Lett.* 1997; 567–568.
11. Kasai PH. *J. Chem. Phys.* 1965; **43**: 3322–3327.
12. (a) Känzig W, Cohen MH. *Phys. Rev. Lett.* 1959; **3**: 509–510; (b) Zeller HR, Kanzig W. *Helv. Phys. Acta* 1967; **40**: 845.
13. Fukuzumi S, Okamoto T. *J. Am. Chem. Soc.* 1993; **115**: 11600–11601.
14. Fukuzumi S, Mochizuki S, Tanaka T. *Inorg. Chem.* 1989; **28**: 2459–2465.
15. Sawyer DT, Calderwood TS, Yamaguchi K, Angelis CT. *Inorg. Chem.* 1983; **22**: 2577–2583.
16. (a) Fukuzumi S. *Bull. Chem. Soc. Jpn.* 1997; **70**: 1–28; (b) Fukuzumi S, Itoh S. *Adv. Photochem.* 1998; **25**: 107–172.
17. (a) Fridovich I. *J. Biol Chem.* 1989; **264**: 7761–7764; (b) Fridovich I. *Annu. Rev. Biochem.* 1995; **64**: 97–112.
18. Bertini I, Banci L, Piccioli M. *Coord. Chem. Rev.* 1990; **100**: 67–103.
19. Tainer JA, Getzoff ED, Richardson JS, Richardson DC. *Nature (London)* 1983; **306**: 284–287.
20. Cass AEG. In *Superoxide Dismutases in Metalloproteins*, Harrison P (ed). Verlag Chemie: Weinheim, 1985; part 1, 121.
21. Ohtsu H, Shimazaki Y, Odani A, Yamauchi O, Mori W, Itoh S, Fukuzumi S. *J. Am. Chem. Soc.* 2000; **122**: 5733–5741.
22. Bencini A, Bertini I, Gatteschi D, Scozzafava A. *Inorg. Chem.* 1978; **17**: 3194.
23. Fridovich I, Beauchamp C. *Anal. Biochem.* 1971; **44**: 276–287.
24. Weser U, Schubotz LM, Lengfelder E. *J. Mol. Catal.* 1981; **13**: 249–261.
25. Tabbi G, Driessen WL, Reedijk J, Bonomo RP, Veldman N, Spek AL. *Inorg. Chem.* 1997; **36**: 1168–1175.
26. Pierre JL, Chautemps P, Refaif S, Beguin C, Marzouki AE, Serratrice G, Saint-Aman E, Rey P. *J. Am. Chem. Soc.* 1995; **117**: 1965–1973.
27. Hart PJ, Balbirnie MM, Ogihara NL, Nersissian AM, Weiss MS, Valentine JS, Eisenberg DA. *Biochemistry* 1999; **38**: 2167–2178.
28. Ohtsu H, Fukuzumi S. *Chem. Eur. J.* 2001; **7**: 4947–4953.

29. Ohtsu H, Fukuzumi S. *Chem. Lett.* 2001; 920–921.
30. Ohtsu H, Fukuzumi S. *Angew. Chem., Int. Ed. Engl.* 2000; **39**: 4537–4539.
31. (a) Page CC, Moser CC, Chen X, Dutton PL. *Nature (London)* 1999; **402**: 47–52; (b) Langen R, Chang IJ, Germanas JP, Richards JH, Winkler JR, Gray HB. *Science* 1995; **268**: 1733–1735; (c) Winkler JR, Gray HB. *Chem. Rev.* 1992; **92**: 369–379.
32. (a) Chambron JC, Chardon-Noblat S, Harriman A, Heitz V, Sauvage JP. *Pure Appl. Chem.* 1993; **65**: 2343–2392; (b) Harriman A, Sauvage JP. *Chem. Soc. Rev.* 1996; **25**: 41–48; (c) Blanco MJ, Jiménez MC, Chambron JC, Heitz V, Linke M, Sauvage JP. *Chem. Soc. Rev.* 1999; **28**: 293–305.
33. (a) Wasielewski MR. In *Photoinduced Electron Transfer*, Fox MA, Chanon M. (eds). Elsevier: Amsterdam, 1988; part A, 161–206; (b) Wasielewski MR. *Chem. Rev.* 1992; **92**: 435–461; (c) Jordan KD, Paddon-Row MN. *Chem. Rev.* 1992; **92**: 395–410.
34. (a) Verhoeven JW. *Pure Appl. Chem.* 1990; **62**: 1585–1596; (b) Verhoeven JW, Scherer T, Willemse RJ. *Pure Appl. Chem.* 1993; **65**: 1717–1722.
35. Fukuzumi S, Imahori H, Yamada H, El-Khouly M, Fujitsuka M, Ito O, Guldi DM. *J. Am. Chem. Soc.* 2001; **123**: 2571–2575.
36. Imahori H, Tamaki K, Guldi DM, Luo C, Fujitsuka M, Ito O, Sakata Y, Fukuzumi S. *J. Am. Chem. Soc.* 2001; **123**: 2607–2617.
37. Fukuzumi S, Guldi DM. In *Electron Transfer in Chemistry*, vol. 2, Balzani V (ed). Wiley-VCH: Weinheim, 2001; 270–337.
38. Fujitsuka M, Ito O, Imahori H, Yamada K, Yamada H, Sakata Y. *Chem. Lett.* 1999; 721–722.
39. Yamada K, Imahori H, Nishimura Y, Yamazaki I, Sakata Y. *Chem. Lett.* 1999; 895–896.
40. Luo C, Guldi DM, Imahori H, Tamaki K, Sakata Y. *J. Am. Chem. Soc.* 2000; **122**: 6535–6551.
41. Imahori H, Guldi DM, Tamaki K, Yoshida Y, Luo C, Sakata Y, Fukuzumi S. *J. Am. Chem. Soc.* 2001; **123**: 6617–6628.
42. (a) Sund H. *Pyridine–Nucleotide Dependent Dehydrogenase*, Walter de Gruyer: Berlin, 1977; (b) Kellogg RM, *Top. Curr. Chem.* 1982, **101**: 111–145.
43. (a) Bunting JW, *Bioorg. Chem.* 1991; **19**: 456–491; (b) He GX, Blasko A, Bruice TC. *Bioorg. Chem.* 1993; **21**: 423–430; (c) Ohno A. *J. Phys. Org. Chem.* 1995; **8**: 567–576.
44. Fukuzumi S. In *Advances in Electron Transfer Chemistry*, vol. 2, Mariano PS (ed). JAI Press: Greenwich, CT, 1992; 67–175.
45. Fukuzumi S, Koumitsu S, Hironaka K, Tanaka T. *J. Am. Chem. Soc.* 1987; **109**: 305–316.
46. Fukuzumi S, Fujii Y, Suenobu T. *J. Am. Chem. Soc.* 2001; **123**: 10191–10199.
47. (a) Fukuzumi S, Nishizawa N, Tanaka T. *J. Chem. Soc., Perkin Trans. 2* 1985; 371–378; (b) Ishikawa M, Fukuzumi S. *J. Chem. Soc., Faraday Trans.* 1990; **86**: 3531–3536.
48. Anne A, Moiroux J, Savéant JM. *J. Am. Chem. Soc.* 1993; **115**: 10224–10230.
49. Takada N, Itoh S, Fukuzumi S. *Chem. Lett.* 1996; 1103–1104.
50. Fukuzumi S, Suenobu T, Patz M, Hirasake T, Itoh S, Fujitsuka M, Ito O. *J. Am. Chem. Soc.* 1998; **120**: 8060–8068.
51. (a) Guldi DM, Kamat PV. In *Fullerenes, Chemistry, Physics, and Technology*, Kadish KM, Ruoff RS (eds). Wiley-Interscience: New York, 2000; 225–281; (b) Guldi DM, Prato M. *Acc. Chem. Res.* 2000; **33**: 695–703.
52. (a) Imahori H, Sakata Y, *Adv. Mater.* 1997; **9**: 537–546; (b) Fukuzumi S, Imahori H. In *Electron Transfer in Chemistry*, vol. 2, Balzani V (ed). Wiley-VCH: Weinheim, 2001; 927–975.
53. (a) Gust D, Moore TA. In *The Porphyrin Handbook*, vol. 8, Kadish KM, Smith KM, Guilard R (eds). Academic Press: San Diego, CA, 2000; 153–190; (b) Gust D, Moore TA, Moore AL. *Acc. Chem. Res.* 2001; **34**: 40–48; (c) Martín N, Sánchez L, Illescas B, Pérez I. *Chem. Rev.* 1998; **98**: 2527–2548; (d) Diederich F, Gómez-López M. *Chem. Soc. Rev.* 1999; **28**: 263–277.
54. Xie Q, Arias F, Echegoyen L. *J. Am. Chem. Soc.* 1993; **115**: 9818–9819.
55. Reed CA, Bolskar RD, *Chem. Rev.* 2000; **100**: 1075–1119.
56. Reed CA, Kim KC, Bolskar RD, Mueller LJ. *Science* 2000; **289**: 101–104.
57. Fukuzumi S, Satoh N, Okamoto T, Yasui K, Suenobu T, Seko Y, Fujitsuka M, Ito O. *J. Am. Chem. Soc.* 2001; **123**: 7756–7766.
58. (a) Fukuzumi S, Kuroda S, Tanaka T. *J. Am. Chem. Soc.* 1985; **107**: 3020–3027; (b) Fukuzumi S, Okamoto T, Otera J. *J. Am. Chem. Soc.* 1994; **116**: 5503–5504.
59. Fukuzumi S, Mori H, Imahori H, Suenobu T, Araki Y, Ito O, Kadish KM. *J. Am. Chem. Soc.* 2001; **123**: 12458–12465.

